Electronic Supporting Information

Increasing Excited State Lifetimes of Cu(I) Coordination Complexes via Strategic Surface Binding

Jiaqi Chen,[a] Henry C. London,[a] Dhruba Pattadar,[b] Charlotte Worster,[c] Sahan R. Salpage ,[a] Elena Jakubikova,[c,*] S. Scott Saavedra,[b,*] Kenneth Hanson[a,*]

[a]Department of Chemistry & Biochemistry, Florida State University, Tallahassee, Florida 32306, United States

[b]Department of Chemistry & Biochemistry, University of Arizona, Tucson, Arizona, 85721, United States

[c]Department of Chemistry, North Carolina State University, Raleigh, North Carolina, 27601, United States

Contents

1. Materials .....Page S3
2. Sample preparation .....Page S3-4
3. Experimental Methods .....Page S4-7
4. **Figure S1**. Absorption spectra for **1** and **2** .....Page S8
5. **Figure S2**. Adsorption isotherms for **1** and **2** .....Page S8
6. **Table S1**. Fitting parameters for **1** and **2** .....Page S8
7. **Figure S3**. TA spectra for ZrO_2-**1**/**2** at 50 % loading .....Page S9
8. **Table S2**. Fitting parameters for ZrO_2-**1**/**2** at 50 % loading .....Page S9
9. **Figure S4**. TA spectra for **1** and **2** in PMMA.....Page S10
10. **Figure S5**. Absorption and TA spectra of **1** and $\mathbf{1_{Et}}$.....Page S10
11. **Figure S6**. Absorption and TA spectra of **2** and $\mathbf{2_{Et}}$.....Page S11
12. **Figure S7**. Absorption spectra of $\mathbf{1_{Et}}$ and $\mathbf{2_{Et}}$ in MeOH and $CHCl_3$ .....Page S11
13. **Figure S8**. TA spectra of $\mathbf{1_{Et}}$ and ZrO_2-**1** in MeOH and $CHCl_3$.....Page S12
14. **Figure S9**. TA spectra of $\mathbf{2_{Et}}$ and ZrO_2-**2** in MeOH and $CHCl_3$.....Page S12
15. **Figure S10**. Molecular orbital energy diagrams .....Page S13
16. **Table S3**. Loading conditions for p-ATR.....Page S13
17. **Table S4.** TD-DFT singlet excited states for structure **1**.....Page S15
18. **Table S5**. TD-DFT singlet excited states for structure **2**.....Page S16

19. **Figure S11.** General depiction of the φ interligand dihedral angle.....Page S17
20. **Figure S12.** Calculated UV-VIS spectra of **1** and **2**.....Page S18
21. **Table S6**. Lowest energy transition dipole orientation .....Page S18
22. **Figure S13.** Visualization of transition dipole moment vectors.....Page S18
23. **Figure S14.** Singly occupied natural orbitals of **1** and **2**.....Page S19
24. **Figure S15.** ATR-IR absorption spectra of **1** and **2** .....Page S19
25. **Figure S16.** Calculated IR spectra of complex **1**.....Page S19
26. **Figure S17.** Calculated IR spectra of complex **2**.....Page S20
27. **Table S7.** Conditions used for ATR measurements .....Page S20
28. **Table S8.** Transition dipole moment tilt angles from ATR.....Page S20
29. **Figure S18.** TM-polarized ATR spectra of **1** on ITO .....Page S21
30. **Figure S19.** TM-polarized ATR spectra of **2** on ITO .....Page S21
31. **Figure S20.** TM-polarized ATR spectra of dextran-fluorescein .....Page S21
32. Synthesis and Characterization of $\mathbf{1}_{\mathbf{Et}}$ and $\mathbf{2}_{\mathbf{Et}}$.....Page S22-25
33. References.....Page S26

Materials

Ethyl 2-methylnicotinate, 10% Palladium on carbon, 6,6′-Dimethyl-2,2′-dipyridyl, 4,4'-di(furan-2-yl)-6,6'-dimethyl-2,2'-bipyridine chloride, tetrakis(acetonitrile)copper(I) hexafluorophosphate, hydrochloric acid, potassium hydroxide, potassium permanganate, sulfuric acid, sodium bicarbonate, copper(II) sulfate, ascorbic acid were purchased from Sigma–Aldrich and used as received. All other reagents and solvents (analytical reagent grade) have been purchased and used without further purification from Alfa Aesar. Glass substrate was obtained from Hartford Glass Co. Meltonix film (1170−25) and the Vac'n Fill Syringe (65209) were purchased from Solaronix. Micro glass cover slides (18 × 18 mm) were purchased from VWR.

Sample Preparation

Solution samples were prepared by dissolving **1** and **2** or **1**-$\mathbf{2_{Et}}$ in anhydrous solvent and bubble deaerating for at least 15 mins. PMMA samples were prepared by dissolving 0.5 wt% PMMA in 3 mL of $CHCl_3$ followed by the addition of 1 mg of $\mathbf{1_{Et}}$ or $\mathbf{2_{Et}}$. The solution was then drop cast on a glass slide followed by slow evaporation. For thin film samples, zirconium oxide nanoparticle paste was prepared using a previously published procedure with minor revision.[1] Briefly, 10 mL of Zirconium (IV) propoxide (70% in n-propanol) was added drop-by-drop at a rate of 30 mL/hr to a stirring solution of 0.42 mL nitric acid in 60 mL deionized water. The resulting solution was continuously stirred for 15 mins followed by heating to 95°C while covered with aluminum foil until the volume was reduced to ~23 mL. The solution was then transferred to a hydrothermal digestion vessel and heated in an oven at 200°C for 10.5 h. Ground carbowax copolymer and water (5% wt) was added to the solution and stirred for 48 h prior to doctorblading.

Metal oxide films were prepared by doctor blading the ZrO_2 paste on an active area of 1 cm^2 (1 layer Scotch tape) on a 2 × 2.5 cm pieces of glass followed by sintering using a previously reported temperature gradient.[2,3] The samples for TA and UV-Vis measurements were loaded by soaking ZrO_2 films in 500 μM solutions of **1** and **2** in MeOH for two hours under nitrogen bubbling. A sandwich cell was then prepared by pressure heating Meltonix films between two

glass slides, one with ZrO_2 and one plain glass. Solvent, either MeOH or $CHCl_3$, was then injected using a Vac'n Fill Syringe and the sample sealed using a Meltonix film and small piece of micro glass cover slide as described previously.[2,3]

Surface Coverages on ZrO_2 (Γ in mol cm^{-2}) were estimated with the expression $\Gamma = (A(\lambda)/\varepsilon(\lambda))/1000$ where ε is the molar extinction coefficient in of complexes in MeOH (9900 for **1** at 483 nm and 8000 M cm^{-1} for **2** at 480 nm) and $A(\lambda)$ is the absorbance at the respective wavelength.[4]

Experimental Methods

Absorption Spectra: Data were recorded on an Agilent 8453 UV-visible photo diode array spectrophotometer. Solution spectra were obtained using a 1 × 1 cm cuvette. Thin film absorption spectra were obtained by placing dry, derivatized ZrO_2 slides or PMMA films perpendicular to the detection of the beam path.

Nuclear Magnetic Resonance (NMR): ^1H data were recorded using Bruker 400 MHz spectrometer were recorded on a Bruker 600 MHz spectrometer at room temperature and all were processed using MNOVA software.

Elemental Analysis: C/H/N elemental analysis were performed via sample submission to Atlantic Microlabs.

High-Resolution Mass Spectrometry (HR-MS): High-resolution mass spectra in MeOH were recorded using an Agilent 6230 TOF MS in positive mode (-ESI).

Attenuated Total Reflectance-Infrared Spectroscopy (ATR-IR): ATR-IR spectra were recorded using a Bruker Alpha FTIR spectrometer (SiC Glowbar source, DTGS detector) with a Platinum ATR quickSnap sampling module (single reflection diamond crystal). Spectra were acquired from 500 to 4000 cm^{-1} at a resolution of 4 cm^{-1}. All ATR-IR spectra are reported in absorbance with a blank versus atmosphere.

Transient Absorption: Transient absorption measurements were performed using a HELIOS FIRE transient absorption spectrometer (Ultrafast Systems) coupled to a Vitara-S Coherent Ti:sapphire laser and amplified using a 1 kHz Coherent Revolution-50 pump laser. The resulting 5 mJ pulse (100 fs full width half max at 800 nm) was then split into a pump and probe beam. The pump was directed through an optical parametric amplifier (OPerA Solo from Coherent). The pump was passed through a chopper to minimize observed laser line scattering. The probe beam was directed through a delay stage and a white light continuum was produced by a sapphire crystal. The pump and probe beam were then overlapped on the sample. For solution measurements, deaerated solvents were used, and continuous stirring was performed on the samples in a 2 mm cuvette during the measurement. For thin films, samples sealed in air-free MeOH or $CHCl_3$ were mounted in a clamp stage. Signal was then collected by a CMOS detector. Difference spectra and single wavelength kinetics were collected averaging 3 times and holding for 2 seconds, with an exponential point acquisition beginning with 0.001 ps steps and totaling to 200 points. Data was processed (chip and time-zero correction) using the Surface Xplorer software package from Ultrafast Systems. Decay kinetics were fit using mono- (equation 1) or biexponential (equation 2) decays with the latter represented by the weighted average (equation 3-5) where the weighting term (W) is dictated by the relative amplitude (A) of the contributors.

$$y = A_1 e^{-(x/t_1)} + y_0 \qquad \text{(eq 1)}$$

$$y = A_1 e^{-(x/t_1)} + A_2 e^{-(x/t_2)} + y_0 \qquad \text{(eq 2)}$$

$$W_1 = (A_1 \times t_1)/(A_1 \times t_1 + A_2 \times t_2) \qquad \text{(eq 3)}$$

$$W_2 = (A_2 \times t_2)/(A_1 \times t_1 + A_2 \times t_2) \qquad \text{(eq 4)}$$

$$\tau = (W_1 \times t_1^2 + W_2 \times t_2^2)/(W_1 \times t_1 + W_2 \times t_2) \qquad \text{(eq 5)}$$

Polarized Visible Attenuated Total Reflectance (p-ATR). p-ATR spectroscopy measurements were performed using a custom-built instrument described in previous publications.[5,6] Briefly, ITO-coated glass slides (Thin Film Devices) were utilized as planar waveguides. A collimated, polarized broadband source (a Xe lamp) was coupled into and out of the waveguide using two

BK7 (n=1.51) prisms. The two prisms were separated by 42 mm which provided eight total internal reflections at the ITO/solution interface. The internal reflection angle was 68°. The outcoupled light from the waveguide was directed into a monochromator (Newport MS260i) and was detected by a CCD (Andor iDus420A).

A liquid flow cell was used to exchange solutions in contact with the ITO surface. Adsorption isotherms of **1** and **2** binding to ITO were measured using transverse magnetic (TM) polarized light and are shown in Figure S17-19. The adsorption isotherms were used to establish conditions for preparing films for molecular orientation measurements. These conditions are given in Table S7. Estimates of the surface coverage of **1** and **2** in monolayer films are given in Table S8. The mean tilt angles of the absorbance dipoles of **1** and **2** in monolayer films were measured using polarized ATR spectroscopy. The method described by Mendes et al. was used to correct for the unequal intensities of the interfacial electric fields in transverse electric (TE) and TM polarizations.[7] In this method, an adsorbed film of chromophores with a random molecular orientation (dextrans labeled with fluorescein) with respect to the ITO surface is used to normalize the electric field intensity differences. The wavelength ranges for the integration of the spectra are given in Table S8.

The surface coverage (Γ) of adsorbed **1-2** films was estimated from[8]**:**

$$\Gamma = A_f\,[1000\,N\,\varepsilon_f\,(I_e/I_i)]^{-1} \qquad (4)$$

where A_f is the absorbance measured in TM polarization, ε_f is the molar absorptivity of the dye at max MLCT peak in solution (9900 and 8000 L mol^{-1} cm^{-1} for **1** and **2**, respectively), N is the number of total internal reflections, and I_e/I_i is evanescent transmitted interfacial intensity per unit incident intensity. I_e/I_i was calculated using the two-phase approximation,[9] using refractive indices of n_1 = 1.36 (for methanol) for the superstrate medium, n_2 = 1.52 for the glass slide, and ignoring the metal oxide layer and the adsorbed molecular film.

Computational Methodology: All structures were optimized with the B3LYP[10–13] functional. Note that while typically it is beneficial to include a dispersion correction in the calculations on Cu complexes[14,15], use of the dispersion for the optimization of structure **2** resulted in a large twist between the pyridine groups of the bpy ligand in disagreement with the available

crystal structure, which also negatively impacted the calculated UV-Vis spectrum of this compound. Therefore, we have opted not to use the dispersion correction in our calculations. An SDD pseudopotential and accompanying basis set was used for Cu,[16,17] while 6-311G* basis set was employed for all other atoms.[18] Structure optimizations were performed using the implicit SMD[19] solvent model (methanol). Frequencies were calculated for all of the optimized structures to verify that the structures were true minima with no imaginary frequencies. Finally, wavefunction stability tests were performed on all complexes to verify the structures had stable wave functions. All DFT calculations were performed with the Gaussian 16 software package[20] Revision A.03. All complexes were optimized in their lowest-energy singlet and triplet electronic states.

TD-DFT at the B3LYP/SDD(Cu),6-311G* level of theory in methanol (SMD) was employed to calculate UV-Vis spectra at the ground-state singlet optimized geometries. Forty lowest-energy excited states were calculated. Excited states with an oscillator strength greater than 0.01 and $\lambda > 300$ nm were analyzed.

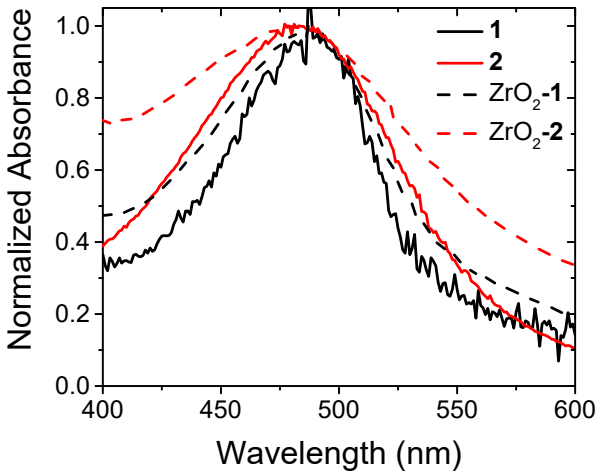

Figure S1. Normalized absorbance spectra for **1** and **2** in MeOH and on ZrO_2.

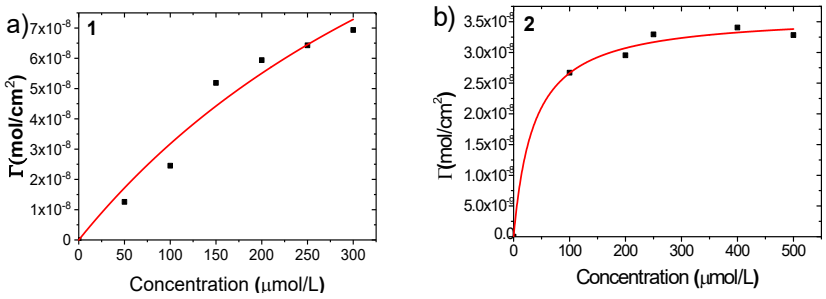

Figure S2. Adsorption isotherms for **1** and **2** in MeOH on ZrO_2.

Table S1. Fitting parameters for the decay kinetics of **1** and **2** solvated and on ZrO_2 in MeOH at various wavelengths.

	λ (nm)	A_1	τ_1 (ps)	A_2	τ_2 (ps)	τ_W (ps)
1	550	1	70	-	-	-
	650	1	85	-	-	-
	690	1	80	-	-	-
	700	1	85	-	-	-
2	550	1	105	-	-	-
	610	1	90	-	-	-
	650	1	90	-	-	-
	700	1	85	-	-	-
ZrO_2-**1**	550	-0.00208	60	-0.00305	495	490
	650	0.00242	45	0.00219	610	610
	690	0.00183	45	0.00171	640	640
	700	0.00165	45	0.00148	595	595
ZrO_2-2	550	0.00258	275	0.00377	2005	1980
	610	0.0061	270	0.00781	1985	1960
	650	0.00488	275	0.00608	2010	1985
	700	0.00258	260	0.00354	1870	1850

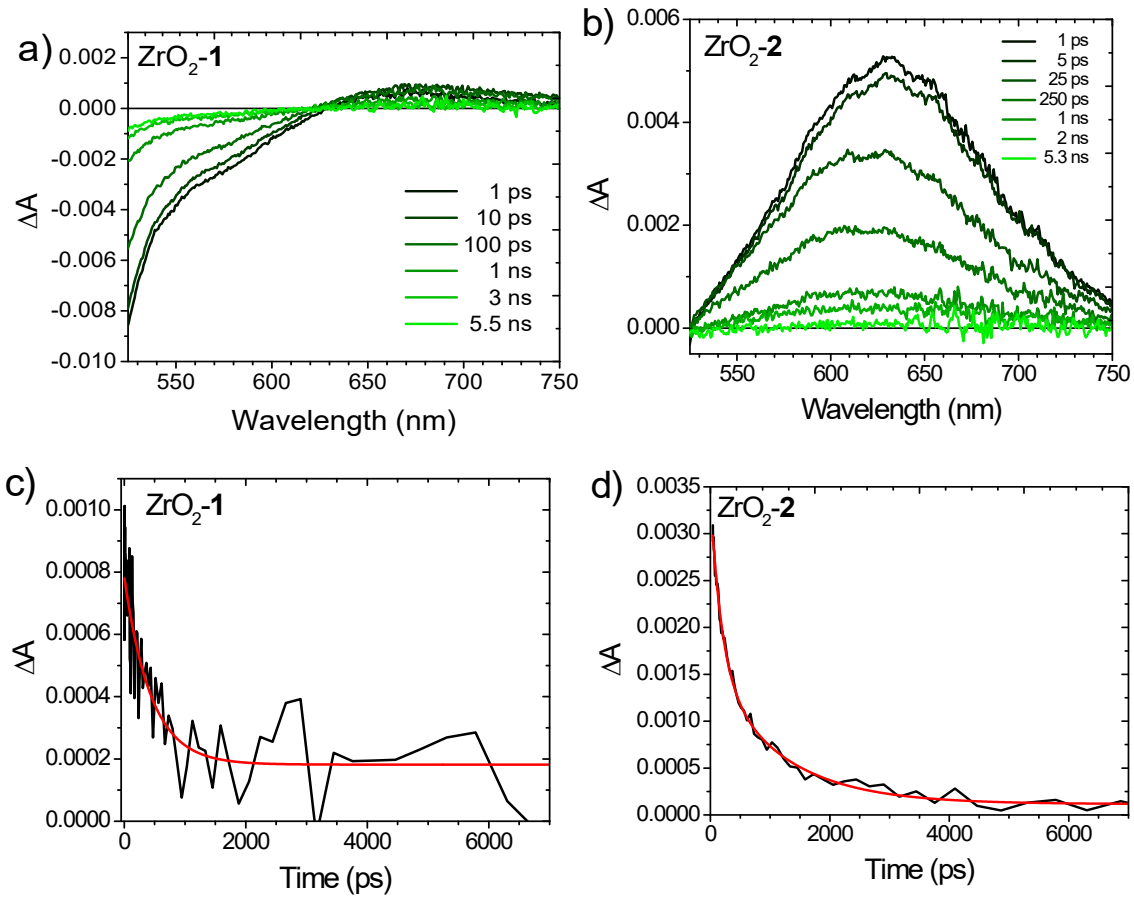

Figure S3. Transient absorption spectra (a and b) and decay traces (c and d) for **1** (a and c) and **2** (b and d) on ZrO_2 at 50% loading in deaerated MeOH. Red lines are for biexponential fits. (λ_{ex} = 500 nm, λ_{abs} = 690 nm for **1** and 610 nm for **2**)

Table S2. Fitting parameters for the decay of **1** and **2** solvated and on ZrO_2 at 50% loading in MeOH (λ_{ex} = 500 nm).

	λ (nm)	A_1	τ_1 (ps)	A_2	τ_2 (ps)	τ_W (ps)
1	690	0.00029	432	0.00029	432	430
2	610	0.00177	184	0.0014	1088	1060

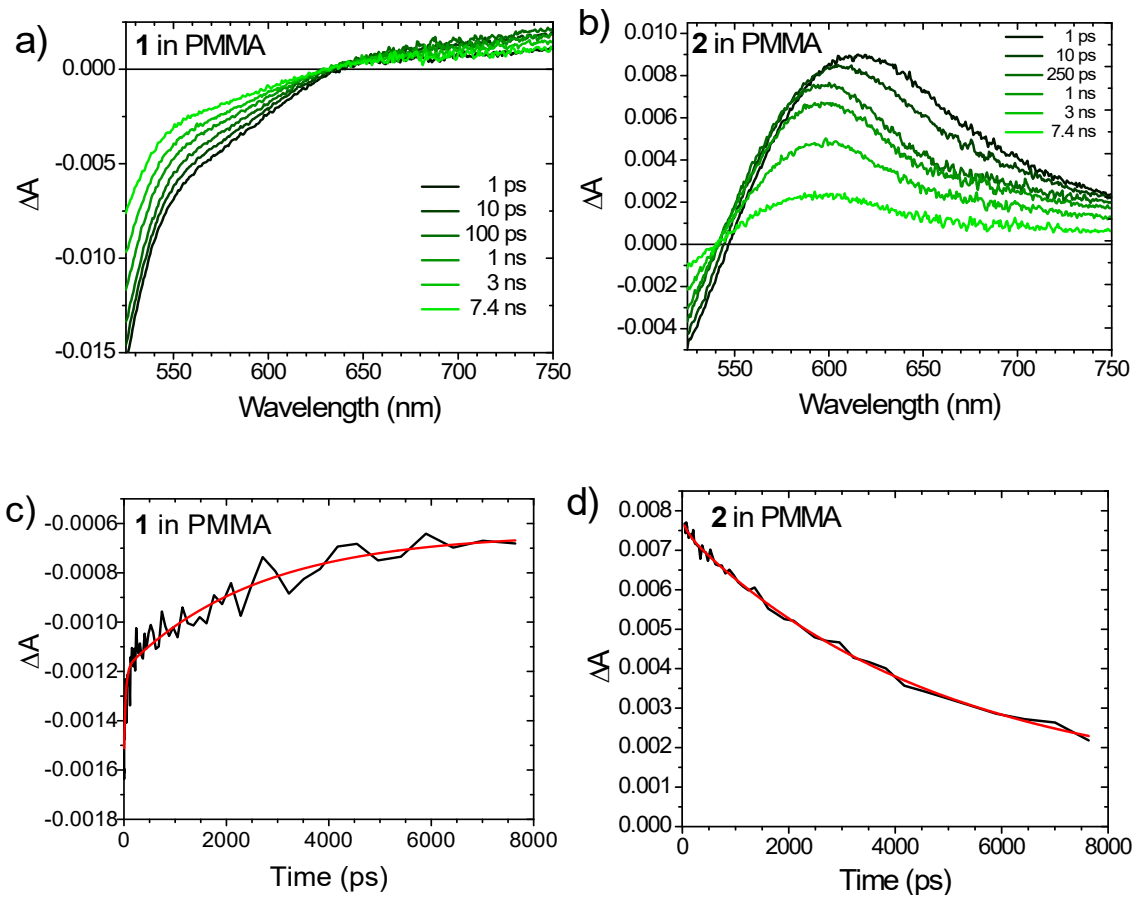

Figure S4. Transient absorption spectra (a and c) and decay traces (c and d) for **1** (a and c) and **2** (b and d) in PMMA. Red lines are for biexponential fits. (λ_{ex} = 500 nm, λ_{abs} = 580 nm for **1** and 610 nm for **2**)

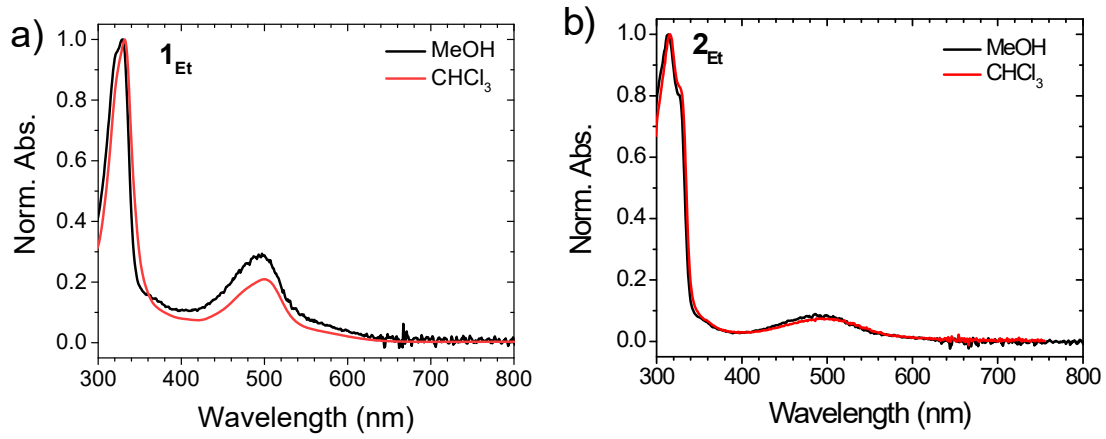

Figure S5. Absorbance spectra of $\mathbf{1}_{Et}$ (a) and $\mathbf{2}_{Et}$ (b) in MeOH and $CHCl_3$.

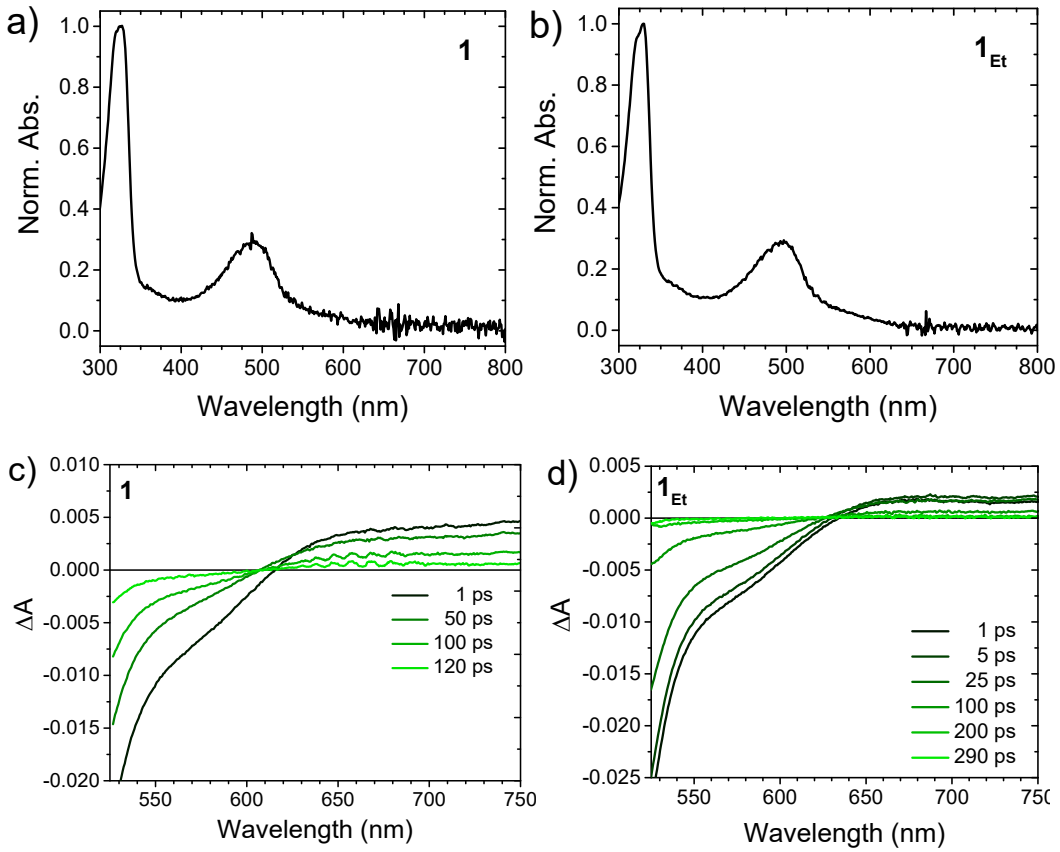

Figure S6. Absorbance (a and b) and TA spectra (c and d) of **1** and $\mathbf{1}_{Et}$ in MeOH (λ_{ex} = 500 nm).

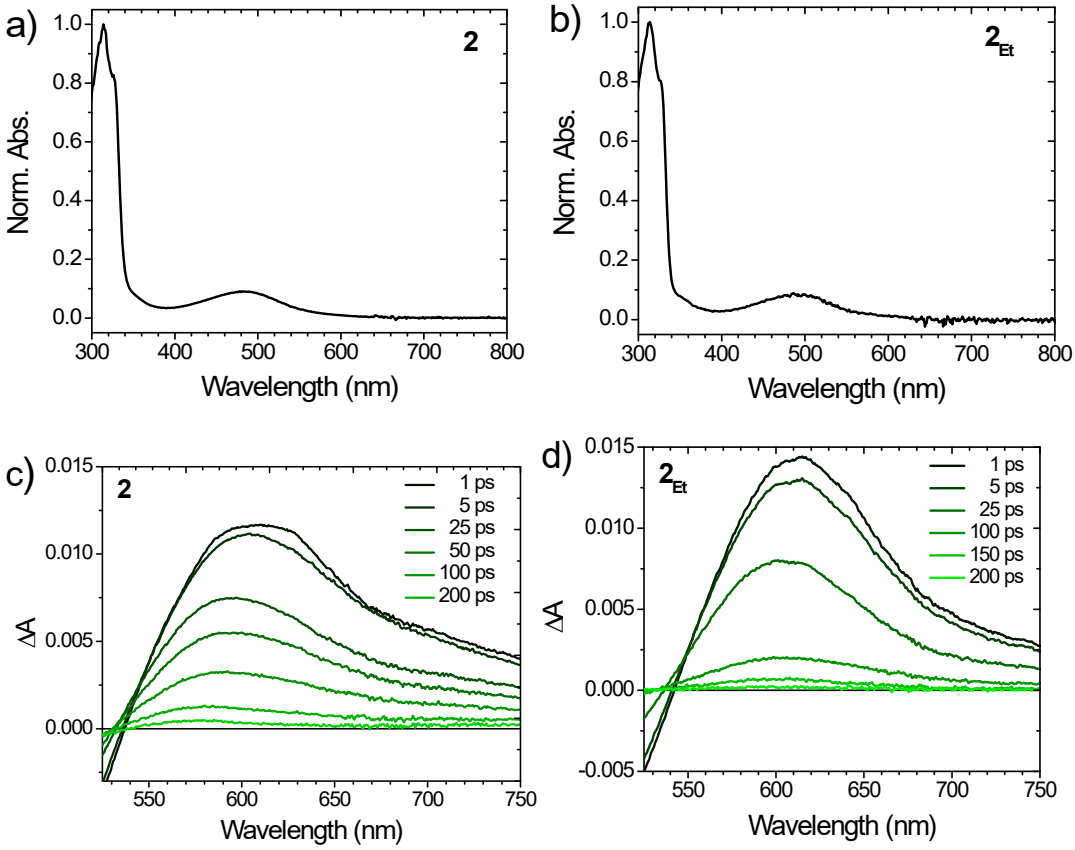

Figure S7. Absorbance (a and b) and TA spectra (c and d) of **2** and $\mathbf{2}_{Et}$ in MeOH (λ_{ex} = 500 nm).

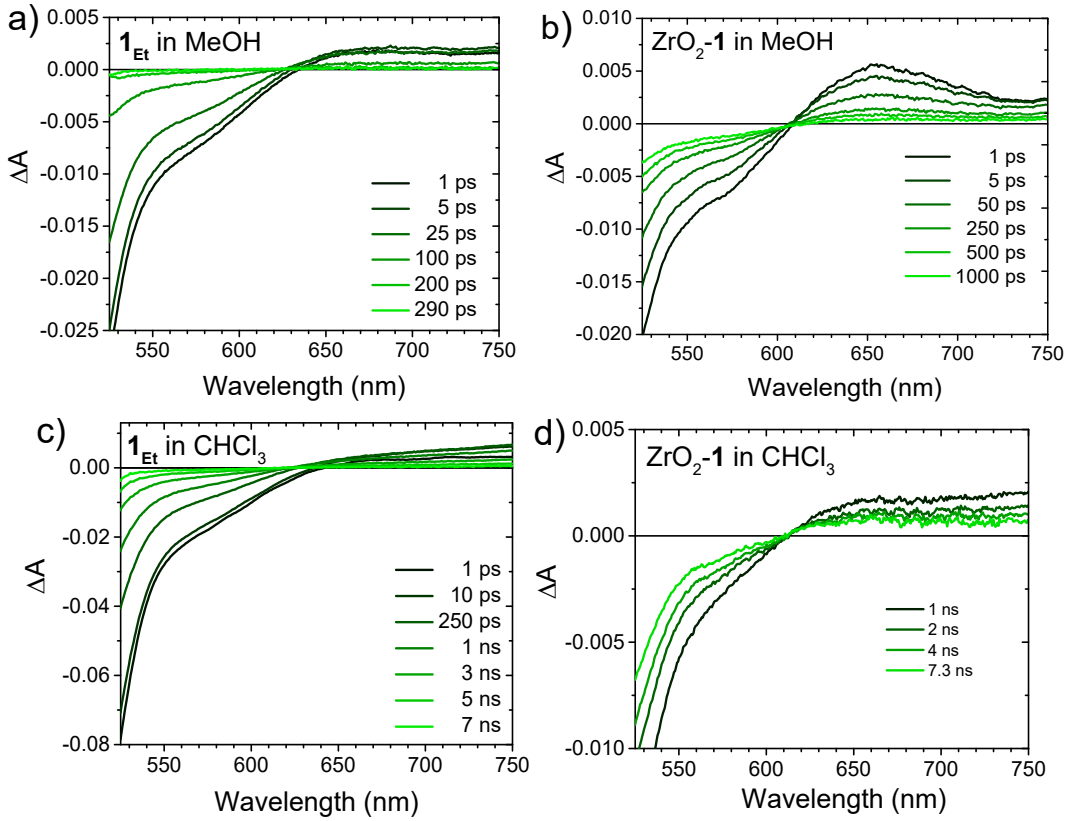

Figure S8. Transient absorption spectra of complex $\mathbf{1}_{Et}$ in MeOH (a) and $CHCl_3$ (c) and ZrO_2-**1** in MeOH (b) and $CHCl_3$ (d). (λ_{ex} = 500 nm)

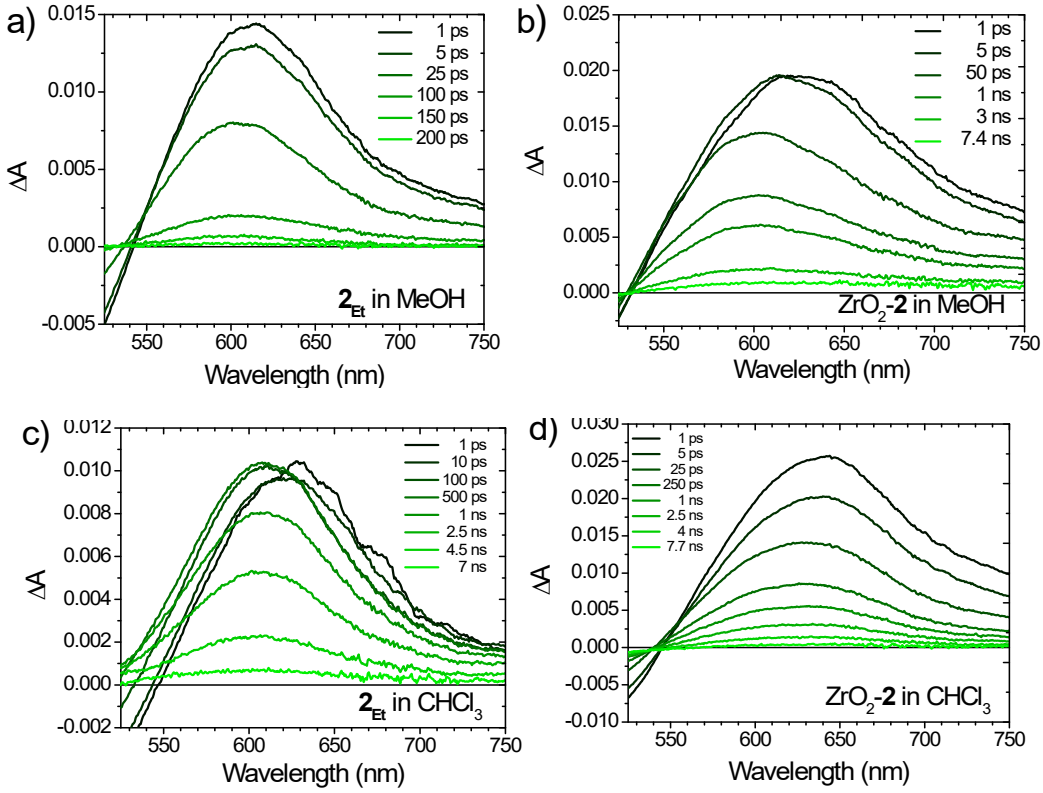

Figure S9. Transient absorption spectra of complex $\mathbf{2}_{Et}$ in MeOH (a) and $CHCl_3$ (c) and ZrO_2-**2** in MeOH (b) and $CHCl_3$ (d). (λ_{ex} = 500 nm)

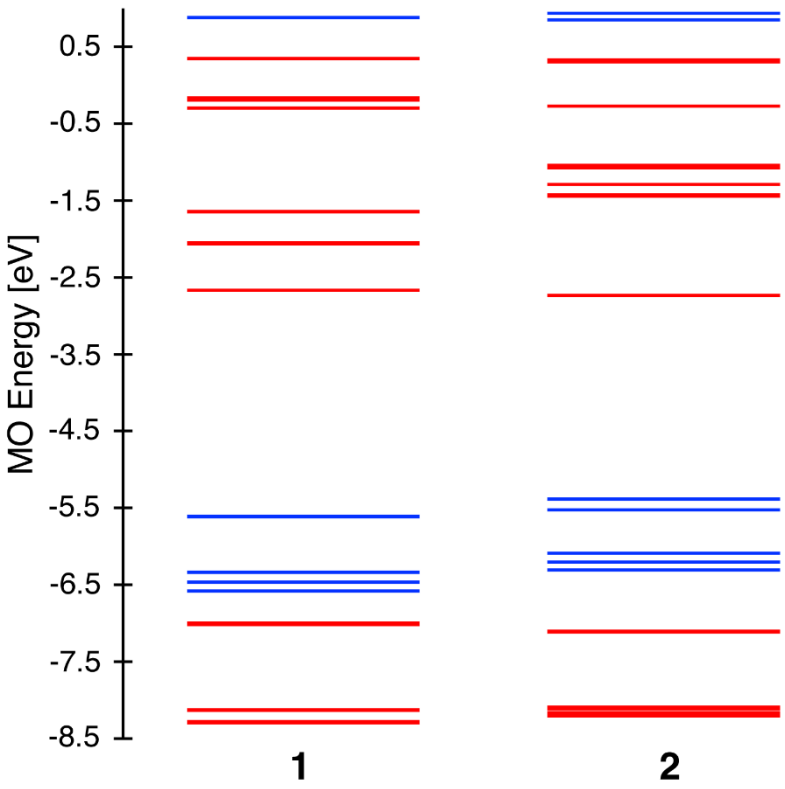

Figure S10. Molecular orbital energy diagrams for **1** and **2**. Ligand- and metal-based orbitals are shown in blue and red, respectively. All orbitals in the energy range between the -8.3 and 1.0 eV are shown.

Table S3. Ground state orbitals HOMO-4 to LUMO+3 of structures **1** and **2**.

Orbital	**1**	**2**
LUMO+3	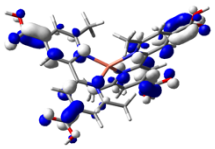	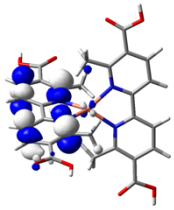
LUMO+2	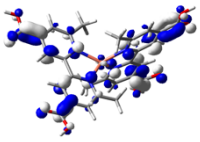	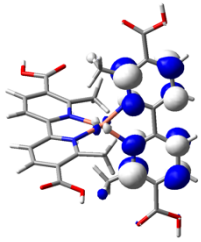

LUMO+1	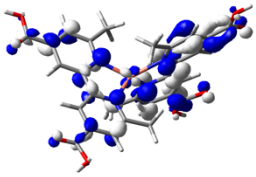	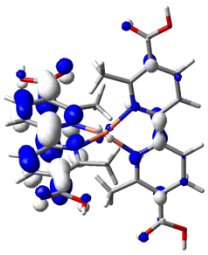
LUMO	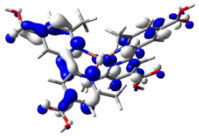	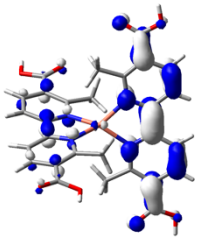
HOMO	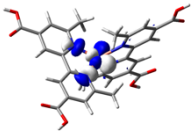	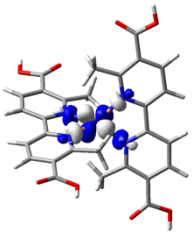
HOMO-1	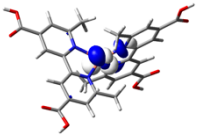	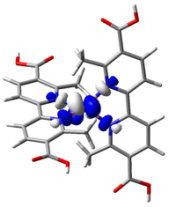
HOMO-2	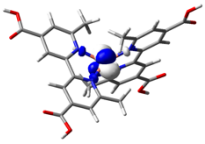	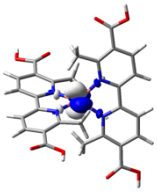
HOMO-3	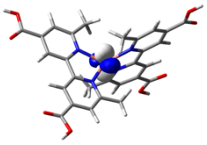	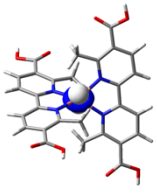
HOMO-4	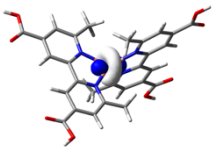	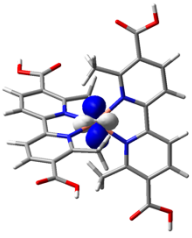

Table S4. TD-DFT singlet excited states for structure **1**. All excited states with an oscillator strength (f_{osc}) > 0.01 and λ > 300 nm were characterized. Only those hole-particle pairs were considered whose contributions add up to ≥ 80%.

Excited State	Excited State Energy and Oscillator Strength	MO Label	Characteristic
3	λ = 2.19 eV = 564 nm f_{osc} = 0.257	HOMO → LUMO HOMO → LUMO+1 HOMO-1 → LUMO HOMO-1 → LUMO+1	MLCT
11	λ = 2.89 eV = 428 nm f_{osc} = 0.027	HOMO → LUMO+2 HOMO → LUMO+3 HOMO-3 → LUMO+1 HOMO-4 → LUMO HOMO-4 → LUMO+1	MLCT
12	λ = 2.90 eV = 427 nm f_{osc} = 0.026	HOMO-4 → LUMO HOMO-4 → LUMO+1 HOMO-3 → LUMO HOMO-1 → LUMO+2 HOMO-1 → LUMO+3	MLCT
13	λ = 2.92 eV = 423 nm f_{osc} = 0.012	HOMO-4 → LUMO HOMO-4 → LUMO+1 HOMO-3 → LUMO HOMO-3 → LUMO+1 HOMO-2 → LUMO HOMO → LUMO+2 HOMO → LUMO+3	MLCT
14	λ = 2.93 eV =423 nm f_{osc} = 0.014	HOMO-4 → LUMO HOMO-4 → LUMO+1 HOMO-3 → LUMO HOMO-3 → LUMO+1 HOMO-2 → LUMO+1 HOMO-1 → LUMO+2 HOMO-1 → LUMO+3	MLCT
17	λ = 3.24 eV = 382 nm f_{osc} = 0.013	HOMO-1 → LUMO+4 HOMO-1 → LUMO+5 HOMO → LUMO+4 HOMO → LUMO+5	LC/MLCT
21	λ = 3.73 eV = 331 nm f_{osc} = 0.089	HOMO-3 → LUMO+3	MLCT
23	λ = 3.78 eV = 328 nm f_{osc} = 0.275	HOMO-6 → LUMO HOMO-6 → LUMO+1 HOMO-5 → LUMO HOMO-3 → LUMO+4	LC/MLCT

24	λ = 3.78 eV = 327 nm f_{osc} = 0.287	HOMO-6 → LUMO HOMO-6 → LUMO+1 HOMO-5 → LUMO HOMO-5 → LUMO+1 HOMO-3 → LUMO+5	MLCT
31	λ = 4.09 eV = 302 nm f_{osc} = 0.082	HOMO-3 → LUMO+4	MLCT

Table S5. TD-DFT singlet excited states for structure **2**. All excited states with an oscillator strength (f_{osc}) > 0.01 were characterized. Only those hole-particle pairs were considered whose contributions add up to ≥ 80%.

Excited State	Excited State Energy and Oscillator Strength	MO Label	Characteristic
1	λ = 1.80 eV = 688 nm f_{osc} = 0.017	HOMO-1 → LUMO HOMO-1 → LUMO+1 HOMO → LUMO	MLCT
3	λ = 2.00 eV = 618 nm f_{osc} = 0.064	HOMO-1→ LUMO HOMO-1 → LUMO+1 HOMO → LUMO	MLCT
11	λ = 3.07 eV = 403 nm f_{osc} = 0.010	HOMO-1 → LUMO+2 HOMO-1 → LUMO+3 HOMO → LUMO+2 HOMO → LUMO+3	MLCT
13	λ = 3.22 eV = 384 nm f_{osc} = 0.073	HOMO-1 → LUMO+2 HOMO-1 → LUMO+3 HOMO → LUMO+2 HOMO → LUMO+3	MLCT
25	λ = 3.81 eV = 324 nm f_{osc} = 0.067	HOMO-6 → LUMO HOMO-5 → LUMO+1 HOMO-3 → LUMO+2 HOMO-3 → LUMO+3 HOMO-4 → LUMO+2 HOMO-4 → LUMO+3	MLCT
26	λ = 3.85 eV = 321 nm f_{osc} = 0.202	HOMO-6 → LUMO+1 HOMO-5 → LUMO HOMO-5 → LUMO+1 HOMO-3 → LUMO+2 HOMO-3 → LUMO+3	MLCT
27	λ = 3.87 eV = 320 nm f_{osc} = 0.031	HOMO-6 → LUMO HOMO-4 → LUMO+2 HOMO-4 → LUMO+3 HOMO-3 → LUMO+2	Mixed
28	λ = 3.90 eV	HOMO-6 → LUMO	Mixed

	= 317 nm f_{osc} = 0.020	HOMO-6 → LUMO+1 HOMO-5 → LUMO HOMO-5 → LUMO+1 HOMO-3 → LUMO+3	
29	λ = 3.92 eV = 315 nm f_{osc} = 0.109	HOMO-6 → LUMO HOMO-6 → LUMO+1 HOMO-5 → LUMO HOMO-5 → LUMO+1 HOMO-4 → LUMO+3 HOMO-3 → LUMO+2	Mixed
30	λ = 3.96 eV = 313 nm f_{osc} = 0.344	HOMO-6 → LUMO HOMO-6 → LUMO+1 HOMO-5 → LUMO+1 HOMO-4 → LUMO+3 HOMO-3 → LUMO+2	Mixed
31	λ = 3.96 eV = 312 nm f_{osc} = 0.425	HOMO-6 → LUMO HOMO-6 → LUMO+1 HOMO-5 → LUMO+1 HOMO-4 → LUMO+2 HOMO-4 → LUMO+3 HOMO-3 → LUMO+2 HOMO-3 → LUMO+3	LMCT/MLCT
32	λ = 4.02 eV = 307 nm f_{osc} = 0.465	HOMO-6 → LUMO+1 HOMO-5 → LUMO HOMO-5 → LUMO+1 HOMO-4 → LUMO+2 HOMO-4 → LUMO+3 HOMO-3 → LUMO+2 HOMO-3 → LUMO+3	LMCT/MLCT

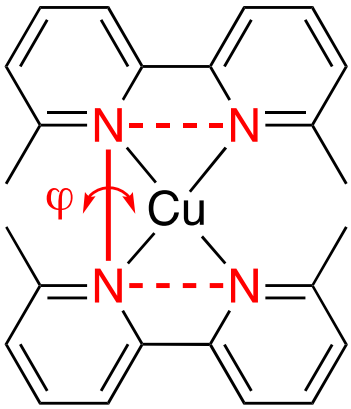

Figure S11. General depiction of the φ interligand dihedral angle for the Cu(I) polypyridyl complexes.

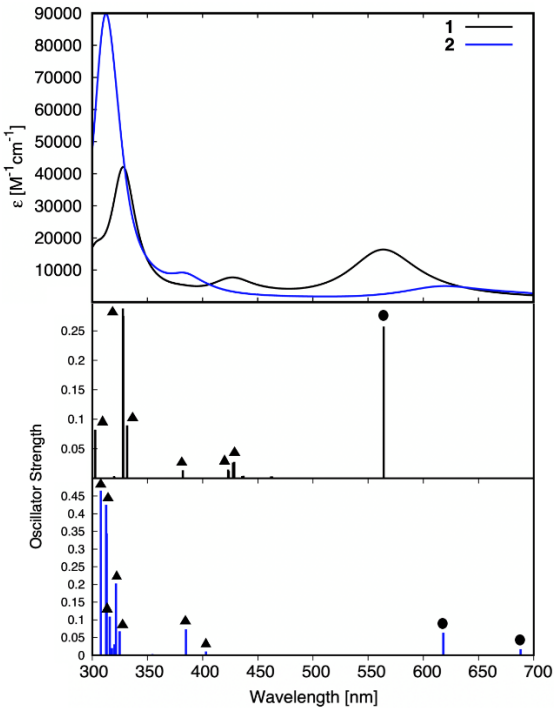

Figure S12. Calculated UV-VIS spectra of **1-2**. States with a circle above them represent MLCT transitions, while triangle states represent LC states.

Table S6. Calculated transition dipoles along with the excitation energies and oscillator strengths for the dominant MLCT transitions.

	X	Y	Z	λ [nm]	Osc. Strength
1	0.036	1.899	-1.082	564	0.574
2	-0.844	-0.038	1.137	618	0.0640

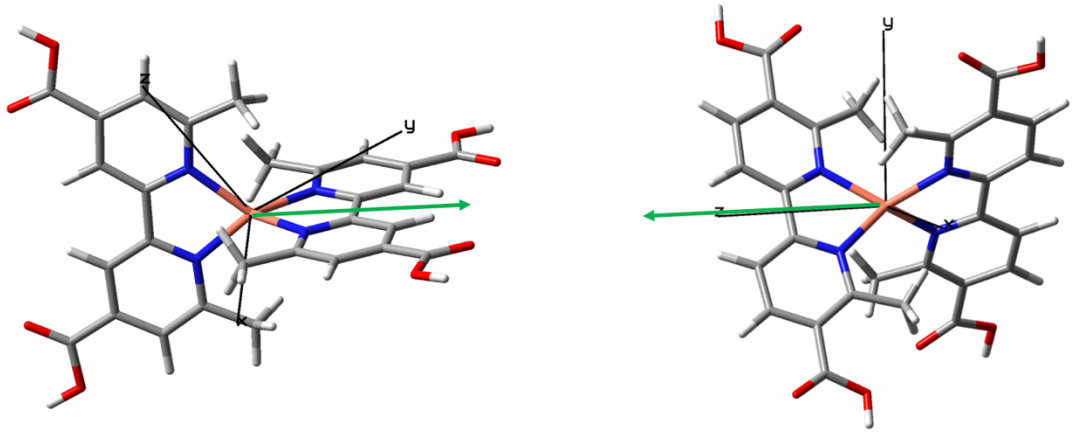

Figure S13. Visualization of transition dipole moment vectors, shown in green originating from the Cu center.

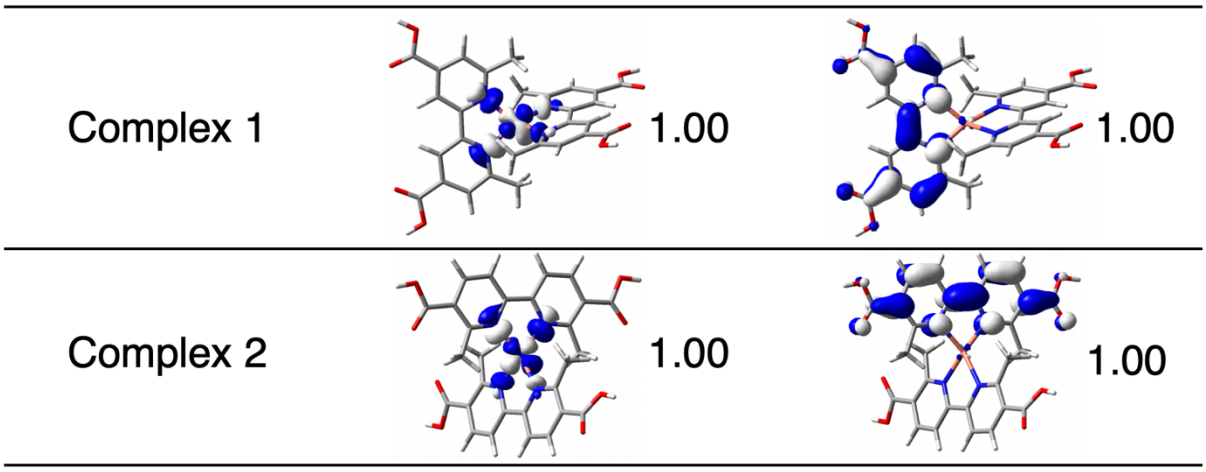

Figure S14. Singly occupied natural orbitals along with their occupation numbers for the lowest energy triplet states of complexes **1** and **2**.

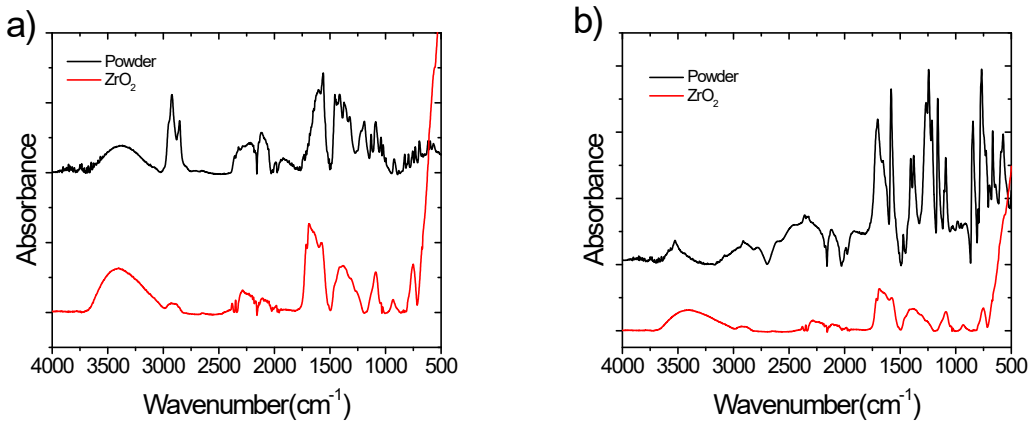

Figure S15. ATR-IR absorbance spectra of neat powder (black) and ZrO_2 bound (red) **1** (a) and **2** (b).

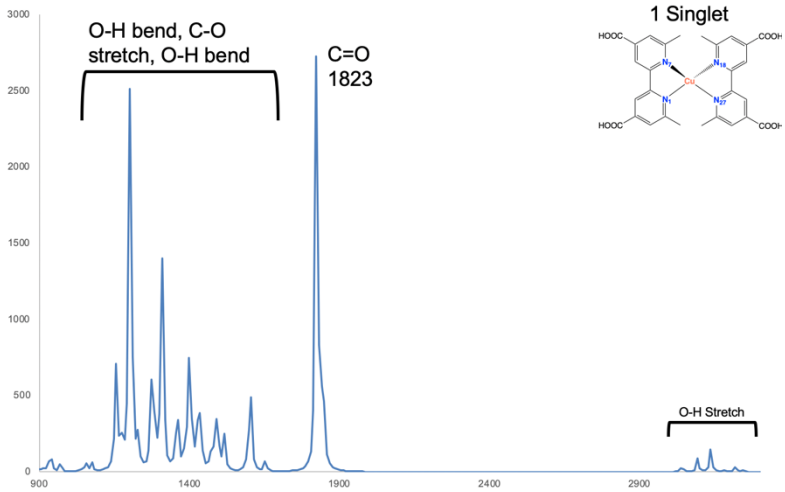

Figure S16. Calculated IR absorbance spectra of complex **1** in the singlet ground state.

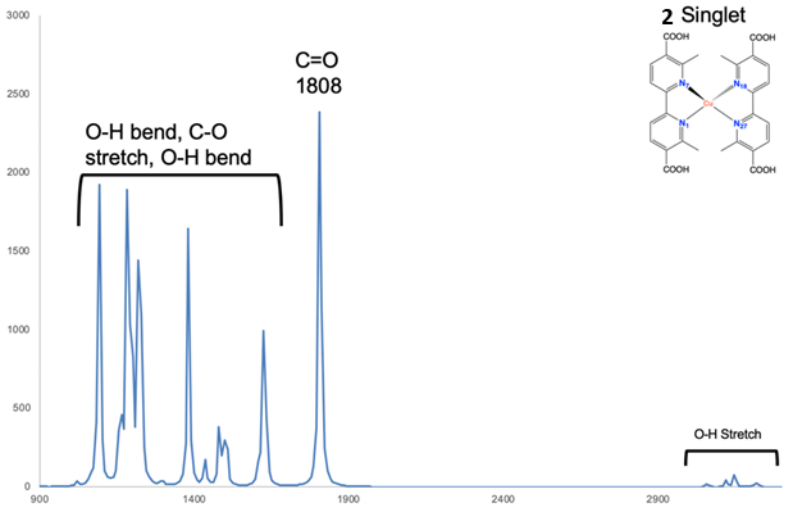

Figure S17. Calculated IR absorbance spectra of complex **2** in the singlet ground state.

Table S7. Conditions used to prepare **1** and **2** on ITO for ATR measurements and Dextran-Fluorescein films for normalization of electric field intensities. The wavelength integration range for each molecule/measurement is also provided.

Species	Conc. (μM)	Solvent	Time (min)	λ integration range (nm)
1	200	Methanol	60	350-575
2	200	Methanol	60	350-575
Dextran-Fluorescein	200	Water	60	400-550

Table S8. Transition dipole moment tilt angles, relative to surface normal, and surface coverage of **1** and **2** on ITO as determined from ATR.

Film	Trial	Tilt angle (deg)	Average Tilt angle (deg)	Surface coverage (mol/cm^2)
1	1	46.9	47 ± 2	1.1 x 10^{-10} (± 0.12)
	2	48.9		
	3	45.4		
2	1	64.2	62 ± 2	9.0 x 10^{-11} (± 2.3)
	2	60.0		
	3	60.0		

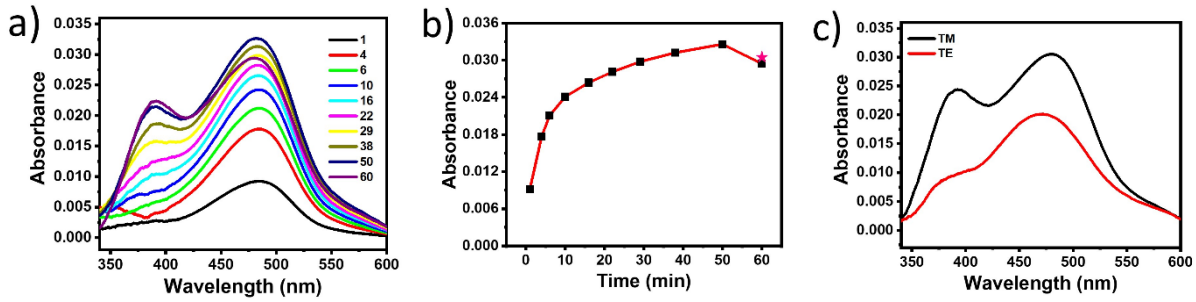

Figure S18. (A) TM-polarized ATR spectra acquired during adsorption of **1** on ITO. The legend indicates the number of minutes that the ITO surface was treated with a 200 μM methanol solution of **1** before the spectrum was acquired. (B) The absorbance at 480 nm vs. time. The pink star is the absorbance after the cell was flushed with fresh methanol. (C) TM- and TE-polarized ATR spectra of the adsorbed **1** film after the cell was flushed with fresh methanol.

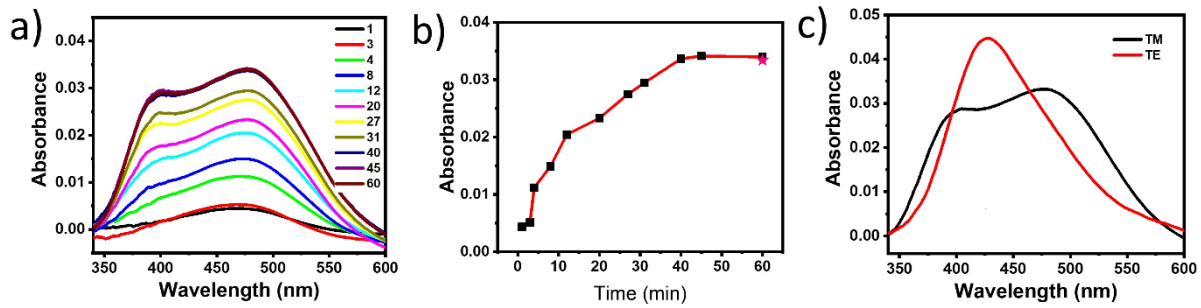

Figure S19. (A) TM-polarized ATR spectra acquired during adsorption of **2** on ITO. The legend indicates the number of minutes that the ITO surface was treated with a 200 μM methanol solution of **2** before the spectrum was acquired. (B) The absorbance at 480 nm vs. time. The pink star is the absorbance after the cell was flushed with fresh methanol. (C) TM- and TE-polarized ATR spectra of the adsorbed **2** film after the cell was flushed with fresh methanol.

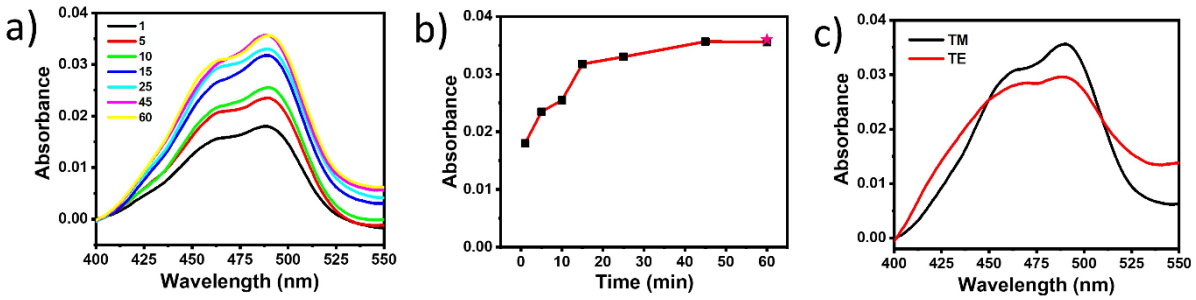

Figure S20. (A) TM-polarized ATR spectra acquired during adsorption of **dextran-fluorescein** on ITO. The legend indicates the number of minutes that the ITO surface was treated with a 200 μM aqueous solution of **dextran-fluorescein** before the spectrum was acquired. (B) The absorbance at 480 nm vs. time. The pink star is the absorbance after the cell was flushed with fresh methanol. (C) TM- and TE-polarized ATR spectra of the adsorbed **dextran-fluorescein** film after the cell was flushed with fresh methanol

Synthesis and Characterization

Complexes **1**, **2**, and their respective ligands were synthesized following previously published procedures.[21,22] Complexes $\mathbf{1_{Et}}$ and $\mathbf{2_{Et}}$ were prepared for the first time as described below.

$\mathbf{1_{ET}}$ (Cu(I)bis(Dimethyl 6,6'-diethyl-[2,2'-bipyridine]-4,4'-dicarboxylate)

Diethyl 6,6'-dimethyl-[2,2'-bipyridine]-4,4'-dicarboxylate (35.9 mg, 0.11 mmol) dissolved in 10 mL MeCN was bubble deaerated with N_2 and then heated to reflux. $Cu(MeCN)_4PF_6$ (18 mg, 0.05 mmol) was then added to the solution which quickly turned dark red. After stirring for 2 hr at reflux, the reaction was cooled to room temperature. After filtration of any residual solid, the filtrate was rotary evaporated until solid. The solid was then dissolved in CH_2Cl_2 and filtered through a plug of silica gel. The resulting solution was evaporated yielding the product as a red solid (35 mg, 44% yield). ^{1}H NMR (600 MHz, $CDCl_3$), δ/ppm: 8.76 (4H, s, H^2), 8.08 (s, 4H, H^5), 4.52 (8H, q, J = 7.1 Hz, H^3), 2.30 (8H, s, H^1), 1.49 (12H, t, J = 7.2 Hz, H^4). ^{13}C NMR (600 MHz, $CDCl_3$), δ/ppm: 164.12, 158.69, 151.98, 140.19, 126.37, 119.55, 62.97, 25.47, 14.37. HRMS: ESI Positive ion mode m/z calcd: 719.2142, found: 719.2276. Found: C, 48.3; H, 4.6; N, 5.9. Calc. for $CuH_{40}C_{36}N_4O_8PF_6 + CH_2Cl_2$: C, 48.3; H, 4.5; N, 6.1.

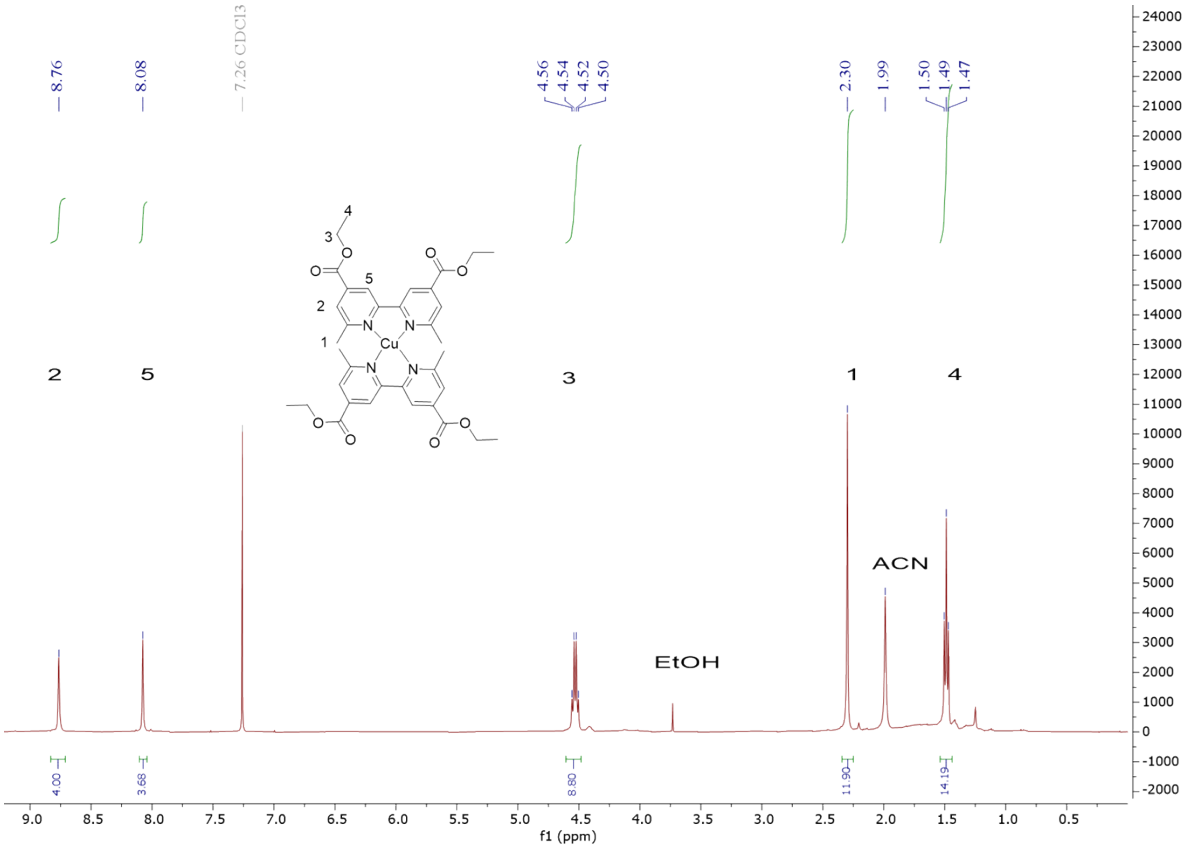

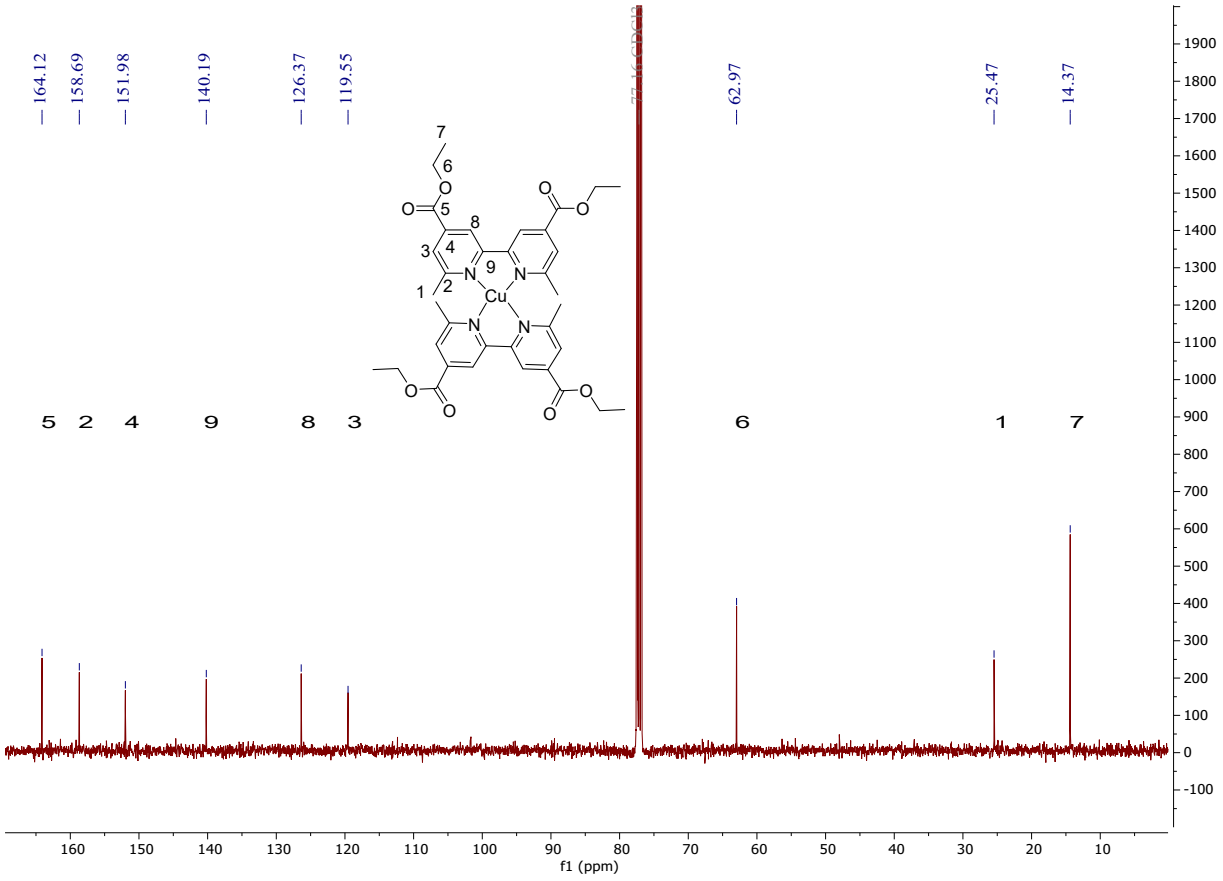
164.12
158.69
151.98
140.19
126.37
119.55
77.16
62.97
25.47
14.37
5 2 4 9 8 3 6 1 7
Cu
N
O
f1 (ppm)

2_{ET} (Cu(I)bis(Dimethyl 6,6'-diethyl-[2,2'-bipyridine]-5,5'-dicarboxylate)

Complex **2** (0.05 g, 0.0822 mmol) was partially disolved in EtOH (10 mL) and then 0.25 mL H_2SO_4 was added. The mixture was refluxed overnight. Upon cooling, the product was extracted with dichloromethane and the organic layer washed with aqueous $NaHCO_3$ and then brine. The organic layer was collected and rotary evaporated to dryness. The resulting solid was then dissolved in $CHCl_3$ and filtered through a plug of silica gel. The resulting solution was evaporated yielding the product as a red solid (0.046 g, 0.0639 mmol). ^{1}H NMR (600 MHz, $CDCl_3$), δ/ppm: 8.39 (4H, d, J = 8.2 Hz, H^5), 8.31 (4H, d, J = 8.2 Hz, H^4), 4.40 (8H, q, J = 7.2 Hz, H^2), 2.91(12H, s, H^1), 1.42 (12H, t, J = 7.2 Hz, H^3). ^{13}C NMR (600 MHz, $CDCl_3$), δ/ppm: 166.74, 159.63, 156.85, 139.53, 125.82, 118.82, 77.37, 77.16, 76.95, 61.44, 25.32, 14.44. HRMS: ESI Positive ion mode m/z calcd: 719.2142, found: 719.2386. Found: C, 44.7; H, 4.4; N, 5.4. Calc. for $CuH_{40}C_{36}N_4O_8PF_6$ + $CHCl_3$: C, 45.1; H, 4.20; N, 5.7.

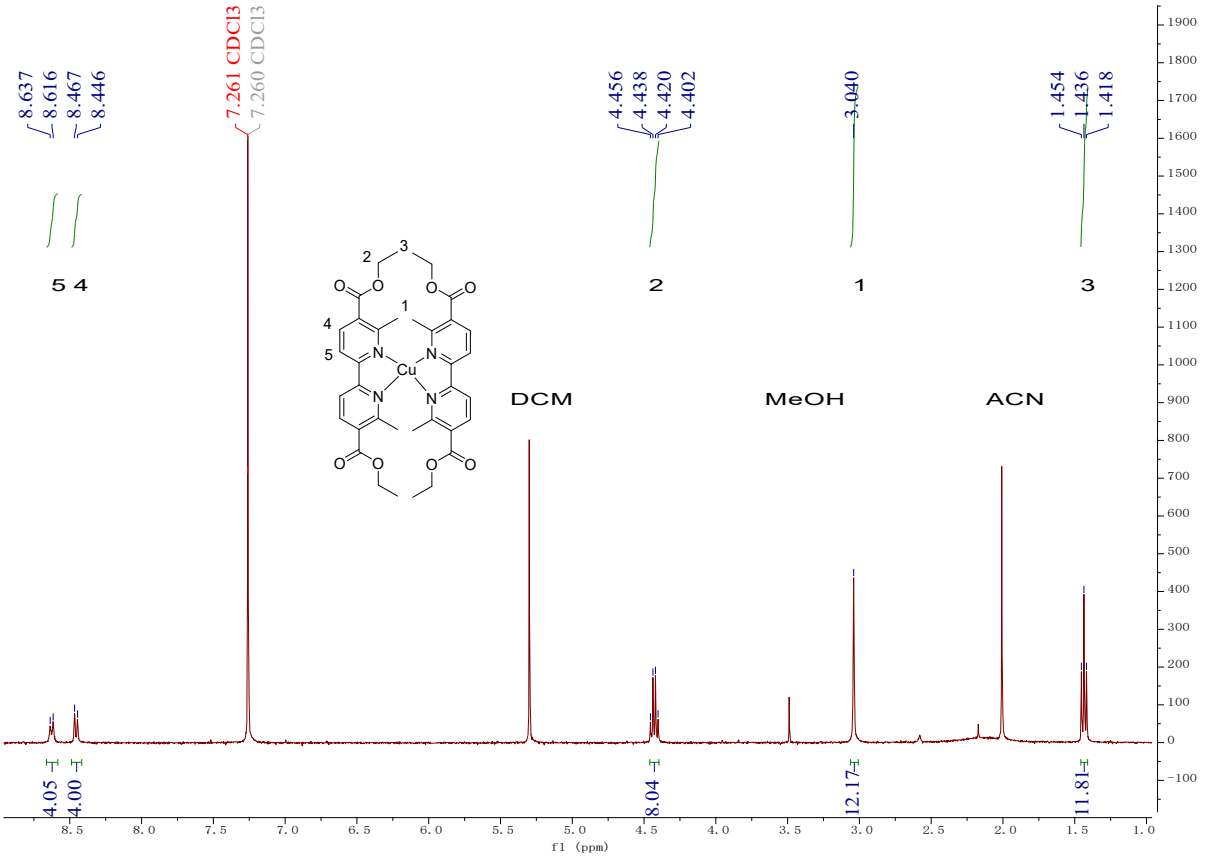

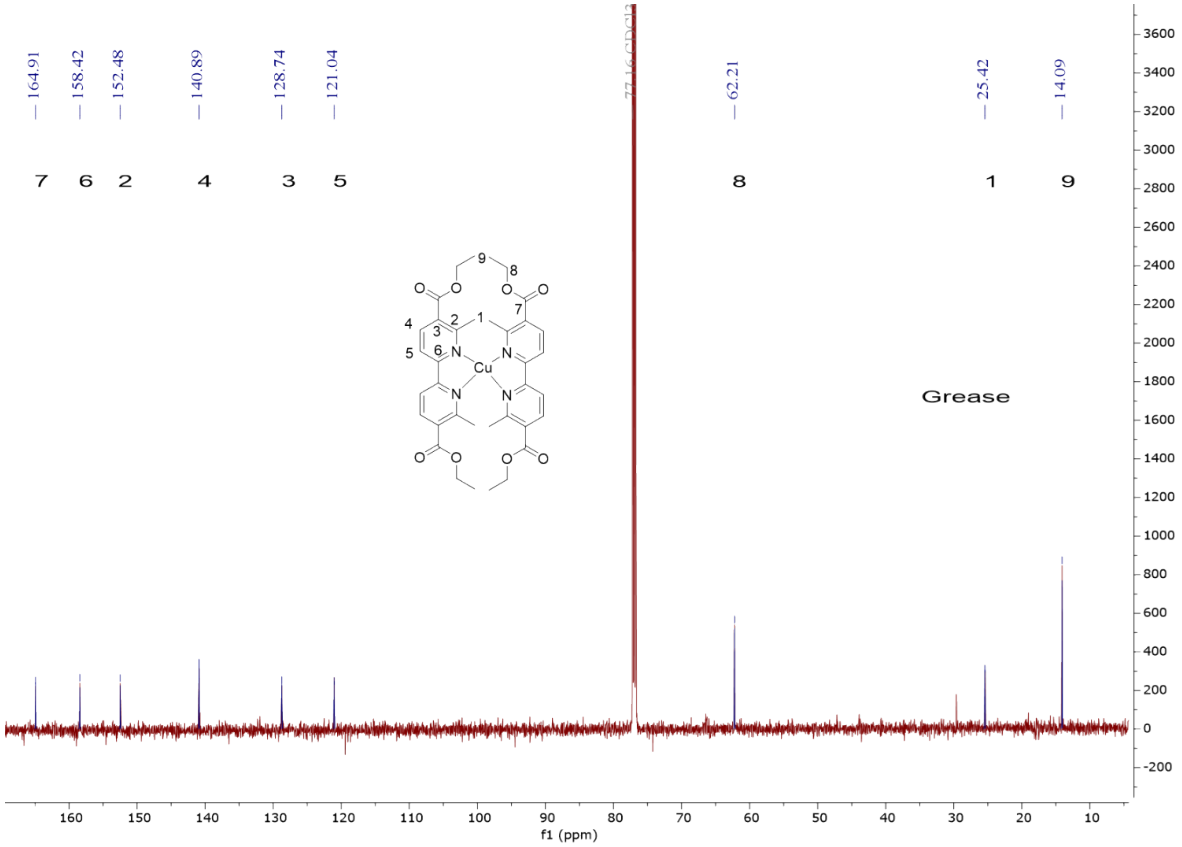
164.91
158.42
152.48
140.89
128.74
121.04
77.16
62.21
25.42
14.09
7
6
2
4
3
5
8
1
9
Grease
f1 (ppm)

References

(1) Heimer, T. A.; D'Arcangelis, S. T.; Farzad, F.; Stipkala, J. M.; Meyer, G. J. An Acetylacetonate-Based Semiconductor−Sensitizer Linkage. *Inorg. Chem.* **1996**, *35* (18), 5319–5324. https://doi.org/10.1021/ic960419j.

(2) Dilbeck, T.; Hill, S. P.; Hanson, K. Harnessing Molecular Photon Upconversion at Sub-Solar Irradiance Using Dual Sensitized Self-Assembled Trilayers. *J. Mater. Chem. A* **2017**, *5* (23), 11652–11660. https://doi.org/10.1039/C7TA00317J.

(3) Hill, S. P.; Dilbeck, T.; Baduell, E.; Hanson, K. Integrated Photon Upconversion Solar Cell via Molecular Self-Assembled Bilayers. *ACS Energy Lett.* **2016**, *1* (1), 3–8. https://doi.org/10.1021/acsenergylett.6b00001.

(4) Langmuir, I. THE ADSORPTION OF GASES ON PLANE SURFACES OF GLASS, MICA AND PLATINUM. *J. Am. Chem. Soc.* **1918**, *40* (9), 1361–1403. https://doi.org/10.1021/ja02242a004.

(5) Araci, Z. O.; Shallcross, C. R.; Armstrong, N. R.; Saavedra, S. S. Potential-Modulated Attenuated Total Reflectance Characterization of Charge Injection Processes in Monolayer-Tethered CdSe Nanocrystals. *J. Phys. Chem. Lett.* **2010**, *1* (12), 1900–1905. https://doi.org/10.1021/jz100475j.

(6) Zheng, Y.; Giordano, A. J.; Shallcross, R. C.; Fleming, S. R.; Barlow, S.; Armstrong, N. R.; Marder, S. R.; Saavedra, S. S. Surface Modification of Indium–Tin Oxide with Functionalized Perylene Diimides: Characterization of Orientation, Electron-Transfer Kinetics and Electronic Structure. *J. Phys. Chem. C* **2016**, *120* (36), 20040–20048. https://doi.org/10.1021/acs.jpcc.6b06812.

(7) Mendes, S. B.; Bradshaw, J. T.; Saavedra, S. S. Technique for Determining the Angular Orientation of Molecules Bound to the Surface of an Arbitrary Planar Optical Waveguide. *Appl. Opt.* **2004**, *43* (1), 70. https://doi.org/10.1364/AO.43.000070.

(8) Saavedra, S. S.; Reichert, W. M. In Situ Quantitation of Protein Adsorption Density by Integrated Optical Waveguide Attenuated Total Reflection Spectrometry. *Langmuir* **1991**, *7* (5), 995–999. https://doi.org/10.1021/la00053a030.

(9) Saavedra, S. S.; Reichert, W. M. Integrated Optical Attenuated Total Reflection Spectrometry of Aqueous Superstrates Using Prism-Coupled Polymer Waveguides. *Anal. Chem.* **1990**, *62* (20), 2251–2256. https://doi.org/10.1021/ac00219a019.

(10) Becke, A. D. Density-Functional Exchange-Energy Approximation with Correct Asymptotic Behavior. *Phys. Rev. A* **1988**, *38* (6), 3098–3100. https://doi.org/10.1103/PhysRevA.38.3098.

(11) Becke, A. D. Density-Functional Thermochemistry. III. The Role of Exact Exchange. *J. Chem. Phys.* **1993**, *98* (7), 5648–5652. https://doi.org/10.1063/1.464913.

(12) Becke, A. D. A New Mixing of Hartree–Fock and Local Density-Functional Theories. *J. Chem. Phys.* **1993**, *98* (2), 1372–1377. https://doi.org/10.1063/1.464304.

(13) Lee, C.; Yang, W.; Parr, R. G. Development of the Colle-Salvetti Correlation-Energy Formula into a Functional of the Electron Density. *Phys. Rev. B* **1988**, *37* (2), 785–789. https://doi.org/10.1103/PhysRevB.37.785.

(14) Rosko, M. C.; Wheeler, J. P.; Alameh, R.; Faulkner, A. P.; Durand, N.; Castellano, F. N. Enhanced Visible Light Absorption in Heteroleptic Cuprous Phenanthrolines. *Inorg.*

Chem. **2024**, *63* (3), 1692–1701. https://doi.org/10.1021/acs.inorgchem.3c04024.
(15) Mara, M. W.; Bowman, D. N.; Buyukcakir, O.; Shelby, M. L.; Haldrup, K.; Huang, J.; Harpham, M. R.; Stickrath, A. B.; Zhang, X.; Stoddart, J. F.; Coskun, A.; Jakubikova, E.; Chen, L. X. Electron Injection from Copper Diimine Sensitizers into TiO_2: Structural Effects and Their Implications for Solar Energy Conversion Devices. *J. Am. Chem. Soc.* **2015**, *137* (30), 9670–9684. https://doi.org/10.1021/jacs.5b04612.
(16) Dolg, M.; Wedig, U.; Stoll, H.; Preuss, H. Energy-adjusted Ab Initio Pseudopotentials for the First Row Transition Elements. *J. Chem. Phys.* **1987**, *86* (2), 866–872. https://doi.org/10.1063/1.452288.
(17) Martin, J. M. L.; Sundermann, A. Correlation Consistent Valence Basis Sets for Use with the Stuttgart–Dresden–Bonn Relativistic Effective Core Potentials: The Atoms Ga–Kr and In–Xe. *J. Chem. Phys.* **2001**, *114* (8), 3408–3420. https://doi.org/10.1063/1.1337864.
(18) Krishnan, R.; Binkley, J. S.; Seeger, R.; Pople, J. A. Self-consistent Molecular Orbital Methods. XX. A Basis Set for Correlated Wave Functions. *J. Chem. Phys.* **1980**, *72* (1), 650–654. https://doi.org/10.1063/1.438955.
(19) Marenich, A. V.; Cramer, C. J.; Truhlar, D. G. Universal Solvation Model Based on Solute Electron Density and on a Continuum Model of the Solvent Defined by the Bulk Dielectric Constant and Atomic Surface Tensions. *J. Phys. Chem. B* **2009**, *113* (18), 6378–6396. https://doi.org/10.1021/jp810292n.
(20) 16. Frisch, M. J.; Trucks, G. W.; Schlegel, H. B.; Scuseria, G. E.; Robb, M. A.; Cheeseman, J. R.; Scalmani, G.; Barone, V.; Petersson, G. A.; Nakatsuji, H.; Li, X.; Caricato, M.; Marenich, A. V.; Bloino, J.; Janesko, B. G.; Gomperts, R.; Mennucci, B.; Hratchian, H. P.; Ortiz, J. V.; Izmaylov, A. F.; Sonnenberg, J. L.; Williams; Ding, F.; Lipparini, F.; Egidi, F.; Goings, J.; Peng, B.; Petrone, A.; Henderson, T.; Ranasinghe, D.; Zakrzewski, V. G.; Gao, J.; Rega, N.; Zheng, G.; Liang, W.; Hada, M.; Ehara, M.; Toyota, K.; Fukuda, R.; Hasegawa, J.; Ishida, M.; Nakajima, T.; Honda, Y.; Kitao, O.; Nakai, H.; Vreven, T.; Throssell, K.; Montgomery Jr., J. A.; Peralta, J. E.; Ogliaro, F.; Bearpark, M. J.; Heyd, J. J.; Brothers, E. N.; Kudin, K. N.; Staroverov, V. N.; Keith, T. A.; Kobayashi, R.; Normand, J.; Raghavachari, K.; Rendell, A. P.; Burant, J. C.; Iyengar, S. S.; Tomasi, J.; Cossi, M.; Millam, J. M.; Klene, M.; Adamo, C.; Cammi, R.; Ochterski, J. W.; Martin, R. L.; Morokuma, K.; Farkas, O.; Foresman, J. B.; Fox, D. J. Gaussian 16 Rev. C.01, Wallingford, CT, 2016.
(21) Constable, E. C.; Redondo, A. H.; Housecroft, C. E.; Neuburger, M.; Schaffner, S. Copper(i) Complexes of 6,6′-Disubstituted 2,2′-Bipyridine Dicarboxylic Acids: New Complexes for Incorporation into Copper-Based Dye Sensitized Solar Cells (DSCs). *J. Chem. Soc. Dalton Trans.* **2009**, No. 33, 6634–6644. https://doi.org/10.1039/b901346f.
(22) Bozic-Weber, B.; Constable, E. C.; Housecroft, C. E.; Neuburger, M.; Price, J. R. Sticky Complexes: Carboxylic Acid-Functionalized N-Phenylpyridin-2-Ylmethanimine Ligands as Anchoring Domains for Copper and Ruthenium Dye-Sensitized Solar Cells. *Dalton Trans.* **2010**, *39* (15), 3585. https://doi.org/10.1039/b925623g.